An illustrated anatomical ontology of the developing mouse lower urogenital tract

Supplementary material

Kylie M. Georgas, Jane Armstrong, Janet R. Keast, Christine E. Larkins, Kirk M. McHugh, E. Michelle Southard-Smith, Martin J. Cohn, Ekatherina Batourina, Hanbin Dan, Kerry Schneider, Dennis P. Buehler, Carrie B. Wiese, Jane Brennan, Jamie A. Davies, Simon D. Harding, Richard A. Baldock, Melissa H. Little, Chad M. Vezina and Cathy Mendelsohn.

DETAILED METHODS AND MATERIALS

Modifications to the GUDMAP ontology

The ontology was written as a partonomic, hierarchical ontology to describe the subcompartments of the developing murine UGT (Little et al., 2007). The ontology uses Theiler staging (TS) to define developmental time, with modifications to the lower UGT ontology being made between TS18 (10.5dpc) and TS28 (representing the adult but defined as postnatal day 4 onwards). The original published UGT ontology listed anatomical terms for each TS separately, with every term appended with a unique stage-specific numerical identifier (EMAP:ID). An "abstract" (non-stage-specific) version of the ontology has subsequently been developed (Hayamizu et al., 2013). Here anatomical terms are given an EMAPA:ID with a TS range, indicating the developmental time frame that the term is present. The abstract ontology includes the introduction of the "is-a" relationship; for example nerve of bladder "is-a" nerve of urinary system and "part-of" bladder, together with the removal of the "group" relationship.

The modified version of the ontology is stored as an OBO formatted file, allowing it to be handled by text-editing software. The open source, Java-based ontology editor OBO-Edit2 was used to view the OBO file and make modifications to the ontology (Day-Richter et al., 2007). Editorial control of the revision process has been implemented, with version monitoring being provided by a Git revision control system (https://github.com/). The ontology is available from the GUDMAP website (http://www.gudmap.org/Resources/Ontology/index.php) and will be published on the Open Biological and Biomedical Ontologies (OBO) web resource (http://www.obofoundry.org/). Definitions of anatomical terms in the lower urogenital tract ontology, including defining features, synonyms, molecular markers and lineage relationships where established, can be found on the GUDMAP website (http://www.gudmap.org/Resources/Ontology/index.php) and also downloaded by following the Link to associated supplementary ontology documents.

Mouse strains

All procedures involving animals were approved by the appropriate institutional animal ethics committees, including; Animal Ethics Committee of the University of Melbourne and compliance with the Australian Code of Practice for the Care and Use of Animals for Scientific Purposes (NHMRC); Institutional Animal Care and Use Committee at Vanderbilt University; the University of Florida Institutional Animal Care and Use Committee; University of Wisconsin-Madison Animal Care and Use Committee; and the Institutional animal care and use committee of Columbia University. Mice were housed and bred in controlled animal facilities at each of the institutions, where the humidity, temperature and light/dark periods were kept constant. Animals were allowed access to food and water ad libitum. Transgenic mouse strains used (Supplementary Table 1) have been described previously (Ahn et al., 2004; Gandhi et al., 2013; Harfe et al., 2004; Rosselot et al., 2010; Seifert et al., 2008; Soriano, 1999; Srinivas et al., 1999; Sun et al., 2000).

Collection and processing of tissues

Embryos collected for whole-mount *lacZ* staining (Figures 2 and 3) were fixed for 1hour in 4% paraformaldehyde (PFA) at room temperature or overnight at 4°C in 0.2% PFA. In Figure 9M, Q-S, tissues for cryo-embedding were fixed by immersion in buffered formalin. In Figure 9I-L, N-P, tissues for cryo-embedding were collected after mice were anaesthetised with ketamine and xylazine (100 and 10mg/kg respectively, i.p.) then fixed by intracardiac perfusion with freshly prepared buffered 4% PFA (Kalous et al., 2012). In Figure 9M, adult tissues were collected after transcardiac perfusion and a subsequent 8 hours of fixation at 4°C in neutral buffered formalin. In Figure 9J-L, for adult bladders to be processed as whole mounts, after cervical dislocation, the bladder was removed, briefly rinsed in PBS, then the bladder was cut open along the dorsal midline, pinned flat and slightly

stretched in a dish lined with silicon polymer, then fixed by immersion in 4% PFA as above. E17 tissues, were dehydrated into 100% methanol post-fixation. For sectioning, tissues were embedded in paraffin or frozen in OCT and sectioned at various thicknesses (5-20µm) or embedded in 3% agarose and vibratome-sectioned (100-150µm). Paraffin sections were deparaffinised with Histoclear and rehydrated via an ethanol-series. Cryosections were prepared for immunolabelling by removing OCT by washing in PBS.

For Haematoxylin and eosin stained E17.5 sections in Figure 3U-V, sectioned CD1 females were crossed to males carrying the *ShhGFPcre;R26RlacZ* allele. Embryos were fixed overnight in 4% PFA and dehydrated through a graded ethanol series (25-50-75-100%) followed by Xylene washes. The embryos were incubated in 2 changes of paraffin wax at 55°C under vacuum. The embryos were then embedded in paraffin wax and sectioned at 10µm. Sections were dewaxed in Xylene, rehydrated through ethanol, stained with Harris haematoxylin and Eosin-Y, and finally dehydrated before mounting in Cytoseal.

Wholemount and section immunohistochemisty

For wholemount immunohistochemistry (IHC) of C57BL/6J E17 tissues (Figure 5B, F), labelling was conducted as previously described (Keil et al., 2012). For section IHC of C57BL/6J E17 tissues (Figure 8R), 5µm sagittal sections of paraffin embedded tissues were labelled as described previously (Abler et al., 2011a). For wholemount IHC of E15 bladder-urethra (Figure 9GH), labelling was performed according to methods described previously (Wiese et al., 2012). For whole adult bladders (Figure 9J-L), tissues were immunostained as described previously for studies of whole mount ganglion preparations (Yan and Keast, 2008). All primary antibodies are listed in Table 2.

Section immunofluorescence

For section IF of C57BL/6J fetal tissues at E13 (Figure 1H), E17 (Figure 8R), 5µm sections of paraffin-embedded tissues were labelled as described previously (Abler et al., 2011a). Primary antibodies (Table 2) were followed by species-specific secondary antibodies; Dylight 488 conjugated goat-anti mouse IgG (Jackson ImmunoResearch, #115-487-003, 1:250-500 dilution), Dylight 549 conjugated goat-anti-rabbit IgG (Jackson ImmunoResearch, #115-487-003, 1:500 dilution). For IF of adult tissue shown in Figure 5J: two consecutive 5µm sections are shown, one section was stained with anti-Acta1 mouse monoclonal and DAPI, the other section was stained with anti-Cdh1 rabbit monoclonal and anti-Acta2 mouse monoclonal (see Table 2) and secondary antibodies were Dylight 488 conjugated goat-anti mouse IgG (Jackson ImmunoResearch, #115-487-003, 1:500 dilution), and Dylight 549 conjugated goat-anti-rabbit IgG (Jackson ImmunoResearch, #115-487-003, 1:500 dilution).

For IF of C57BL/6 cryosectioned tissues (Figure 9I, N-P), 14µm cryosections were processed for direct label IF, as described previously (Yan and Keast, 2008). Primary antibodies (Table 2) were detected using species-specific secondary antibodies labelled with fluorophores; Cy3, FITC, AF488 or AF594 (Jackson ImmunoResearch, 1:1000-1:2000 dilution). IF of fetal tissues cryosectioned at 15-20µm (Figure 9Q-S) was performed according to methods described previously, using primary antibodies listed in Table 2 (Wiese et al., 2012).

Section mRNA *in situ* hybridisation

Section mRNA *in situ* hybridisation (SISH) using C57BL/6J E17 tissues (Figure 8P, R), sectioned at 50µm, was conducted as described previously (Abler et al., 2011a, Abler et al., 2011b). Primer sequences used to generate the riboprobe templates were as follows: *Krt14* (nucleotides 1275-1625

of NM_016958.1, 5'-TGCTGGATGTGAAGACAAGG-3' and 5'-CGATGT**TAATACGACTCACTATAGGG**CAGGAAGGACAAGGGTCAAG-3') and *Upk3a* (nucleotides 327 to 933 of NM_023478.2, 5'-TCCCACTGAGCACCACTTTC-3' and 5'-CGATGT**TAATACGACTCACTATAGGG**AGCTTGCTGGAGAACACCTC-3'). Bold, underlined sequences represent a synthetic T7 RNA polymerase binding site incorporated into the PCR primer. Annotated SISH expression patterns for *Krt14* and *Upk3a* are available on the GUDMAP website (www.gudmap.org) with the Accession IDs, GUDMAP:14299 and GUDMAP:14338, respectively. In Figure 8R, IF was performed post-SISH using primary antibodies (Table 2) and secondary antibodies; Fluo-549-labeled polyclonal goat anti-rabbit IgG (Jackson ImmunoResearch Laboratories Inc., 1:500 dilution) and Fluo-488-labeled polyclonal goat anti-mouse IgG (Jackson ImmunoResearch Laboratories Inc., 1:500 dilution), using the IF protocol described above for E17 tissue.

DETAILED LITERATURE REVIEW

Connecting the upper and lower urogenital tract

In the mouse, UGT development begins with formation of the nephric ducts (NDs, also called mesonephric or Wolffian ducts), paired epithelial tubes derived from intermediate mesoderm. From E9-11, the NDs elongate down the embryo and insert into the cloaca, establishing a primary connection between the upper and lower urogenital tract. The cloaca, an epithelial lined cavity derived from endoderm, undergoes septation from E11-13, forming the UGS ventrally and the hindgut dorsally, separated by a strip of mesenchyme called the urorectal septum (URS, Figure 1A-C) (Sasaki et al., 2004; Seifert et al., 2008). Correct cloacal insertion of the NDs is dependent on a number of signalling pathways including *Ret*, *Gata3*, *Retinoids* and *Fgf*, and is crucial to proper positioning of the ureters later in development (Chia et al., 2011; Walker et al., 2013).

Kidney development begins at E10.5, when epithelial ureteric buds (UBs) emerge from the caudal nephric ducts and grow into the adjacent metanephric mesenchyme (MM), in a position anterior to the cloaca. The buds then branch to form a T-shape. Seen at E11.5, the T-shaped UBs are comprised of a ureteric stalk and tips (Figure 1A). Mesenchyme condenses around the tips, forming the cap mesenchyme, the nephron progenitor source during kidney development. Throughout embryogenesis, the ureteric tree will undergo successive rounds of branching morphogenesis to form the renal collecting duct system and renal pelvis of the paired kidneys. The UB stalks will form the ureters, muscular tubes that conduct urine from the renal pelvis to the bladder, where it is stored and excreted. At E11, the UB stalks have not yet established independent insertion sites in the UGS and connect indirectly via the common nephric duct (CND, Figure 1A). The CNDs are defined as the caudal ND segments, below the level of the UB stalk attachment site. From E12-13, the CNDs undergo apoptosis and the ureters make contact with, then merge with the primitive bladder (PBL, Figure 1BC, I-L). As the UGS grows, the ureter orifice moves cranially, while the NDs remain joined to the urogenital sinus ridge (UGS ridge, Figure 1C, L) (Batourina et al., 2005). By E14.5, the ureters and NDs are separated and the CND has regressed (Figure 1M) (Batourina et al., 2005; Mendelsohn, 2009; Viana et al., 2007).

Failure of the ureters to enter the bladder at the correct position can result in urinary obstruction, megaureter and hydronephrosis, or vesicoureteral reflux (Murawski et al., 2008; Wu et al., 2009b). Hydronephrosis commonly results from defective peristalsis (Feeney et al., 2014) or mis-positioned distal ureters, which can be caused by a number of defects including delayed ND insertion (Chia et al., 2011; Walker et al., 2013), abnormal sprouting of the UB (Mackie et al., 1975) or failure in CND remodelling (Batourina et al., 2005; Hoshi et al., 2012; Uetani et al., 2009). Insertion of ureters lateral to the regular insertion site can cause vesicoureteral reflux (Murawski et al., 2007), while insertion at a posterior position, for example in the urethra, can result in urinary obstruction,

impeding the flow of urine from the kidney to the bladder (Hutch, 1972; Tanagho, 1981; Weiss, 1988). Due to the intimate connection with the kidneys, the resulting backflow of urine can lead to hydronephrosis and ultimately renal failure.

Emergence of the genital tubercle and urethral plate epithelium

As occurs in the urinary tract, epithelial-to-mesenchymal interactions play a critical role during genital tubercle (GT) development. *Shh* is expressed by the entire cloacal epithelium and urethral plate epithelium (UPE) and plays a critical role during GT development (Seifert et al., 2010). *Shh* in the UPE regulates gene expression in the adjacent mesenchyme, including *Ptch1, Gli1, Bmp4, Hoxd13*, and *Fgf10* (Haraguchi et al., 2001; Haraguchi et al., 2007; Haraguchi et al., 2000; Lin et al., 2009; Miyagawa et al., 2009; Perriton et al., 2002; Seifert et al., 2009b). *Shh* also promotes GT outgrowth by regulating cell cycle kinetics in GT mesenchyme (Seifert et al., 2010). At E10.5, prior to any obvious GT outgrowth, *Fgf8* is seen at the cloacal membrane, where the surface ectoderm meets the cloacal epithelium (Haraguchi et al., 2001; Haraguchi et al., 2007; Haraguchi et al., 2000; Perriton et al., 2002; Seifert et al., 2009b). Although *Fgf8* has no endogenous role in GT development, its transcription serves as a marker of the endodermal component of the cloacal membrane (Seifert et al., 2009b). Mesenchymal growth from paired ventrolateral genital swellings, which develop in a slightly anterior position adjacent to the cloaca, pushes the epithelial walls of the cloaca together at the cloacal membrane (Perriton et al., 2002). At E11.5, the GT is subdivided into ventrolateral genital swellings and a dorsal genital swelling (Figure 2A) (Perriton et al., 2002; Yamada et al., 2006). At E13, the GT has extended distally out from the embryo and is subdivided into distal (dgt) and proximal (pgt) regions, each comprised of mesenchyme (mpgt/mdgt) and skin (Figure 1C, 2C), and two laterally-positioned preputial swellings (pps, Figure 2C).

Growth from the urorectal septum completely separates the hindgut and UGS. In mice, the urorectal septum is marked by strong *Bmp7* expression, and persistent cloaca and rectourethral fistula are seen in *Bmp7* null embryos (Wu et al., 2009a). In humans, we refer to the skin between the urethral opening and the anus as the perineum. In the mouse, rupturing of the cloacal membrane exposes the terminus of the urorectal septum, which is covered by cloacal endoderm-derived epithelium, between the urethral and hindgut openings (proximal urethral meatus and anus) (Seifert et al., 2008). Consequently, the cloacal endoderm overlying the urorectal septum forms the midline of the perineum, and in mice, is marked by the *Shh+* endodermal cell lineage (Figure 1C) and β-catenin expression (Figure 1H). The skin on either side of the perineum midline is however, surface ectoderm derived (Figure 1C) (Seifert et al., 2008). Endodermally-derived cells remain on the perineum surface until P0, although whether they persist or are replaced after birth remains to be determined.

At E13, the UPE has begun to canalise into a tube (urethral tube epithelium, UTE), forming the phallic urethra (PHUR, Figure 1C). Canalisation is aided by mesenchymal growth from the base of the GT, which surrounds the tube. This mesenchyme is sometimes referred to as the urethral folds. The PHUR epithelium is proximo-distally patterned throughout development. The UPE and UTE show varying degrees of differentiation and different gene expression patterns (Suzuki et al., 2008). *Fgf8* becomes restricted to the growing distal tip, where *Shh* and *Bmp7* are also strongly expressed (Haraguchi et al., 2001; Haraguchi et al., 2000; Perriton et al., 2002; Seifert et al., 2009a; Suzuki et al., 2003).

Updated anatomy of the postnatal mouse penis and clitoris

The postnatal structure of the mouse penis and clitoris has recently been revisited (Rodriguez et al., 2012; Rodriguez et al., 2011; Schlomer et al., 2013; Weiss et al., 2012) and comparisons between human and mouse have been reviewed (Cohn, 2011; Yamada et al., 2003; Yamada et al., 2006). In humans, external genitalia sexual differentiation is completed early in the second trimester (Siiteri et al., 1974; Sinisi et al., 2003; Yiee et al., 2010). In mice however, even at birth, male and female external genitalia are more similar than in humans, both morphologically and morphometrically (Schlomer et al., 2013). Sexual differentiation in mice begins at E15.5 and continues postnatally, such that by 10 days after birth, males and females are quite different and begin to resemble the adult anatomy (Schlomer et al., 2013; Weiss et al., 2012). By 21 days, dramatic differences are seen between the sexes indicating that a significant amount of sexual differentiation occurs after birth in mice. Eight diagnostic anatomical features distinguishable in the adult mouse penis/clitoris have been described (Yang et al., 2010) and sex differences have been examined in the neonatal period (Schlomer et al., 2013) and adult (Weiss et al., 2012).

In males, the penis is subdivided into the glans penis and body of penis (Figure 3W-Y). The penile urethra (PNUR) lies ventrally along the length of the penis and below it lies the corpus cavernosum urethra, erectile tissue (Figure 3W-Y). The penile body also contains two lateral paired bands of erectile tissues, the corpora cavernosa (also called crura; or crus, singular) which attach to the pubic bone (Figure 3W-Y) (Rodriguez et al., 2011). From the body of the penis, the PNUR makes a right angle bend as it extends into the glans penis and it opens at the urethral meatus, located near the distal tip of the penis (Figure 3WY). Proximal to the male urogenital mating protuberance (MUMP), the glandular ridge encircles the glans and contains two linear corpora cavernosa glandis, which run ventrally and dorsally along the glans (Figure 3W-Y). The os penis is a ~3.8mm long bone (although its size is variable) surrounded by hyaline cartilage that lies in the centre of the glans above the

urethra, and overlaps the proximal end of the MUMP (Figure 3W-Y). Cartilage undergoes calcification to form the os penis bone at around 6 months of age. The MUMP is comprised of a cartilage core surrounded by corpus cavernosum and covered with skin and its boundary (red dotted line, Figure 3W-X) is defined by the MUMP ridge, a groove that encircles the distal glans penis. Externally, the preputial seam can be seen as a ventral cleft in the prepuce, extending from the urethral meatus to the tip of the glans penis, where it meets the MUMP. This cleft in the prepuce, which results from preputial fusion, is different to the seam along the ventral side of the glans penis, which is a remnant of the UPE.

The morphology of the adult penis and clitoris can be disrupted when the balance between androgen and estrogen action is altered during late prenatal or postnatal development. Changes to the shape and size of the external genitalia, MUMP size, amount of bone, cartilage and erectile tissue and other features, have all been shown to be influenced by changes in androgen and estrogen action in mice (Blaschko et al., 2013; Yang et al., 2010; Yucel et al., 2003). These changes can lead to abnormal morphology of the external genitalia, feminisation of males and masculinisation of females.

Sexual differentiation of the reproductive ducts and their connection to the pelvic urethra

At E15.5, in both sexes, the caudal ends of the paramesonephric ducts (PNDs, or Mullerian ducts) have laterally fused and the NDs remain connected to the PLUR at the urogenital sinus ridge (UGS ridge, Figure 2E, Figure 4A-B, E) (Iizuka-Kogo et al., 2007). However, the production of Anti-Mullerian Hormone by the testes has already initiated PND degeneration in males. PND degeneration, regulated by β-catenin signalling, progresses in a rostral-to-caudal wave (Figure 4A). Conversely in females, the NDs (also known as mesonephric or Wolffian ducts) degenerate in a

similar directional pattern (Figure 4E). Mesonephric tubules (mt) also degenerate in females (Figure 4E). By E16.5, sex-specific duct degeneration is almost complete, with only remnants of the ducts seen in both sexes (Figure 4C, F) (Iizuka-Kogo et al., 2007).

In developing female mice, the fused caudal portion of the PNDs becomes the upper vagina (UV), eventually becoming the adult vagina (Kurita, 2010). The oviducts, uterus and uterine horn are also derived from the PNDs. *Lhx1* is required in the PND epithelium for normal female development (Huang et al., 2014) and failure of the PNDs to either elongate or fuse can result in congenital absence or duplication of vagina, cervix and uterus, respectively, such as seen in *Dlgh1* KO mice (Iizuka-Kogo et al., 2007). At E16, the female UGS ridge becomes the sinovaginal bulb (SVB, Figure 4F). As development progresses, the SVB separates from the PLUR and the fused UV-SVB extends along the urethra in a caudal direction towards the clitoris (Figure 4F-G). At birth, the vagina is closed and the UV remains internally fused to the urethral epithelium via the SVB. When the SVB reaches the base of the clitoris by P8 (Kurita, 2010), it separates from the urethra, however, because the SVB is a solid epithelial cord, the vagina remains closed. It opens later during puberty, at approximately P28, via an apoptosis dependent process, which can be prevented by the overexpression of *Bcl2* (Kurita, 2010; Rodriguez et al., 1997). In the adult, the entire vaginal epithelium is derived from *Hoxb7-Cre* expressing PND epithelia and does not contain cells derived from the UGS, UGS ridge or NDs (Kurita, 2010). Vulvar epithelium does contain cells derived from UGS and it is thought that during vaginal opening, the remaining SVB epithelial cells become part of the vulvar epithelium (Kurita, 2010).

During development, the anterior reproductive ducts differentiate into other components of the reproductive system; in females, anterior PNDs will become the oviducts, connecting the uterus to the ovaries, and in males the anterior NDs will become the epididymis, while the cranial

mesonephric tubules will become the efferent ducts, completing the connection between the ductus deferens and the testes.

Morphological sex differences in the pelvic urethra

During PLUR development, three distinct clusters of condensed mesenchyme form at the bladder neck-urethra junction, centred on the midline at sites where the prostate buds develop in the male (Figure 4D, Figure 5A-B). These mesenchymal pads, seen from E17 to birth, are thought to play a role in bud differentiation (Timms et al., 1995). Females also develop mesenchymal pads though they are smaller and more elongated than the male (Figure 5E) (Abler et al., 2011). Mesenchymal pads of both sexes are subdivided into dorsal, ventral and lateral (Figure 5A, E). All pads are marked by F*gf10*, while *Scmh1* specifically marks the male and female ventral mesenchymal pads (Abler et al., 2011).

In the E17 male PLUR, the lamina propria and submucosa layers are thicker, whilst the female has a thicker muscle layer, which is also continuous with the detrusor muscle of the female bladder, where there is a large gap in males (Figure 5A-C, E-G) (Abler et al., 2011). The angle the PLUR connects to the bladder also differs between sexes. Seen at a right angle in males, and more linear in females, the angle is prominent at E17 and is maintained in the adult (Figure 5A, E, I', K'). As development progresses, continued sex-specific differentiation eventually results in an adult urethra that is highly sexually dimorphic (Figure 5I-N). This reflects the dual function of the male urethra in the transit of semen and urine from the body. The male urethra is much longer than the female as it extends into the penis (penile urethra, PNUR) (Yamada et al., 2003; Yang et al., 2010). As a result of development of the prostate gland and seminal vesicles, both contributing to seminal fluid, the adult male urethra is divided into the prostatic, pelvic and penile urethra (PRUR, PLUR, PNUR respectively; Figure 3Y).

The ejaculatory duct openings also located in the prostatic urethra and connect the seminal vesicles and testes, via the ductus deferens, to the urethra (Figure 5A-D, I-J).

Prostate gland anatomy and development

The anatomy of the adult prostate and its terminology has a confusing history (Timms, 2008). The adult mouse prostate is positioned at the bladder-urethra junction and surrounds the PRUR and ejaculatory ducts (Figure 5I-J). Unlike the human prostate, which is bounded distally by a thick fibromuscular capsule and divided into anatomical zones, the mouse prostate is subdivided into four bilaterally symmetrical regions (historically known as lobes); anterior, dorsal, lateral and ventral (Figure 5A-B, D, I). Each region has its own distinct morphology and function, specified during development via both common and region-specific genetic pathways (Cunha et al., 1987; Donjacour et al., 1987).

At E16.5, anterior and dorsal prostatic buds are the first to emerge, followed by lateral and ventral buds at E17 (Figure 5A-B). The buds emerge from the epithelium in response to androgen-induced paracrine-acting signals from the surrounding mesenchyme (Cunha et al., 1987). Buds are comprised of peri-prostatic mesenchyme and epithelium that is exclusively marked by *Wnt10b*, *Edar* and *Nkx3-1* in all four regions (Abler et al., 2011; Allgeier et al., 2008; Keil et al., 2012). *Bmp2* is selectively expressed by ventral prostatic buds (Abler et al., 2011) and loss of *Wnt5a* selectively inhibits ventral bud development (Allgeier et al., 2008).

Urethral gland development

Urethral gland buds are evident at E18 and are more numerous in males than females (Allgeier et al., 2008). In males, they are especially concentrated in the PLUR segment bounded cranially by the

ejaculatory ducts and caudally by the bulbourethral glands. In male mice at birth, urethral gland buds are usually distinguishable from the more developed, longer prostate gland buds. Newborn males have developed numerous urethral gland buds along the length of the PLUR (Figure 5D), however only ventral epithelial buds are seen in females (Figure 5H) (Allgeier et al., 2010). Female ventral epithelial buds are more numerous than those seen in the male, however they are short, only a few cells in diameter and uniformly distributed (Figure 5H'). In contrast, male ventral buds include two rows of longer ventral prostate buds and fewer, centrally positioned smaller ventral epithelial buds (Figure 5D') (Allgeier et al., 2010). Adult female urethral glands, also called Skene's glands, have been described in other rodents and in humans (Biancardi et al., 2010; Fochi et al., 2008; Wernert et al., 1992; Zaviacic et al., 2000). However in mice, little is known about the origin of these or the fate of the female ventral epithelial buds. Although a careful time course analysis to precisely determine their fate in adults has not been performed, it is likely that these buds become the urethral glands that are evident in the adult (Figure 5L-N, Figure 6L).

The bladder trigone

Trigone development is important for normal bladder function. As the bladder fills and pressure increases, the distal ureter segments (intravesicular, Figure 6D) that pass through the bladder wall are compressed, preventing backflow of urine to the kidneys (vesicoureteral reflux). This is commonly referred to as the anti-reflux valve. The trigone is first established at E13.5, when the ureter opens directly into the bladder lumen (Figure 1C, L). Although the trigone was initially thought to differentiate from the CND (Hutch, 1972; Mackie et al., 1975; Tanagho, 1981; Tanagho et al., 1968), lineage analysis has shown that the epithelial portion of the trigone derives from the UGS (Seifert et al., 2008). The muscular portion, which gives the trigone its distinct triangular structure (illustrated in Figure 6E-F) derives from intersecting detrusor and longitudinal ureteral muscle fibers (Figure 6K-L) (Viana et al., 2007). In the adult, the trigone urothelium has a smooth luminal surface,

in contrast to the folded surface seen in the rest of the bladder (see Figure 5M, Figure 7K), most likely due to the underlying muscular structure.

The ureters

The ureters are lined by a urothelium, comprised of superficial, intermediate and basal cell layers, and Uroplakin expression is seen along their length (Figure 6G-J). Superficial cells lining the lumen, intermediate cells and Krt5-expressing basal cells are seen in the ureter urothelium, however the layers are not subdivided into cell types in the ontology. Within the baldder trigone, the muscle layer of the ureters is distinct from that of the detrusor (Batourina et al., 2005; Viana et al., 2007). Interestingly, unlike the bladder, ureteral smooth muscle differentiation does not occur until E15 and progresses in a rostro-caudal wave beginning at the pelvic junction (Carpenter et al., 2012). Most of the ureters are encased by 2-3 layers of circular and longitudinal smuscle fibers, which are important for conducting peristaltic waves to propel urine from the renal pelvis to the bladder (Figure 6G-L). On the other hand, the muscle layer of the distal-most ureteral segment passing through the bladder wall contains only a thin layer of longitudinal fibers, a configuration that may be important for efficient compression and function of the anti-reflux valve (Figure 6K).

The bladder urothelium

The bladder urothelium differentiates into a highly specialized water-tight barrier that prevents exchange of water and toxic substances between the blood and urine (Hu et al., 2002; Khandelwal et al., 2009). The urothelium is one of the most quiescent epithelia in the body, but can rapidly regenerate in response to injury from urinary tract infection or toxins (Jost, 1986). Chronic irritation or injury can compromise barrier function leading to bladder pain disease and voiding dysfunction (Birder, 2011; Birder et al., 2007; Wyndaele et al., 2003).

Cell types in the urothelium of the bladder can be identified by their protein expression profiles (Gandhi et al., 2013) and relative positions in the urothelial cell layers (C.M., unpublished data illustrated in Figure 8A-F). From E11-E12, very few undifferentiated epithelial cells, expressing endodermal markers (Trp63, Krt5, Foxa2, Shh, Isl1) but not Upk, are seen in the primitive bladder urothelium, usually at the luminal surface. Although at these stages, most of the primitive bladder is lined by P-0 cells, a transient progenitor cell population expressing Trp63, Krt5, Foxa2, Shh, Isl1 and Upk, but not Krt5 (Figure 8A-B, G). However, by E13, intermediate cells (ICs; Upk^{+} $Trp63^{+}$ Shh^{+} $Foxa2^{-}$ Isl^{-} $Krt5^{-}$) make up most of the primitive bladder urothelium (Figure 8CH). At E14, the basal cell layer of the bladder urothelium is lined with ICs and the superficial layer is composed of superficial cells (SCs, or immature umbrella cells) which are Upk^{+} $Trp63^{-}$ Shh^{-} $Foxa2^{-}$ Isl^{-} $Krt5^{-}$ (Figure 8D, J). Superficial cells (SCs, also called umbrella cells) are specialized for the synthesis and transport of uroplakins, which assemble into the crystalline plaque that serves as the urothelial barrier (Khandelwal et al., 2009; Kong et al., 2004; Romih et al., 2005). Unlike their mature counterparts, an enormous, multinucleated population, immature SCs (or immature umbrella cells) are mononucleated and similar in size to other urothelial cell types. By E18, SCs are polyploid and resemble mature SCs (or mature umbrella cells, Figure 8N) (Romih et al., 2005). Fully-differentiated SCs uniquely express Krt20, from E18 to adult (see Figure 8T) (Erman et al., 2006). Krt5-expressing basal cells (K5-BCs; Krt5+, Shh+, Upk-, Isl1-, Foxa2-) are first observed in the basal layer at E14. By E15, K5-BCs populate most, if not all, of the basal layer and can also be found in the intermediate layers, interspersed with ICs (Figure 8D-F, L-N). By E17 and in the adult, Krt5-BCs line the entire basal cell layer and the intermediate cell layer remains a mixture of Krt5-BCs and ICs (Figure 8E, F, N).

Nerves and vasculature of the lower urogenital tract

Bladder nerves and vasculature have been described more thoroughly in adult rats (Gabella, 1995, 1999; Gabella et al., 1998; Inoue et al., 1991). The development of these structures during mouse embryogenesis has not been extensively characterized and the stage when urethral tissues are first innervated has not been determined, it is known that axonal processes have penetrated the bladder wall by E14 (Wiese et al., 2012). We do know that bladder innervation is well developed in the mouse by birth (Levin et al., 2007; Yan et al., 2008). This contrasts with the reproductive organs that show little or no innervation at birth, but in which nerves continue to mature until puberty (Keast, 2006; Yan et al., 2008).

Arterial and venous vessels, components of the vasculature, are found on the serosal and adventitial surface of the bladder and urethra, and continue to branch as they pass through the muscle and lamina propria layers (Figure 9A-FL). A complex vascular network lies close to the basal surface of the urethral epithelium and bladder urothelium (Figure 9LM). Although studies examining the architecture and morphology of vasculature in the adult mouse bladder have recently been performed (Hashitani et al., 2012; Hossler et al., 2013), vascular development in foetal mice is poorly understood.

Within the bladder wall, nerve fibres (axons) are present throughout each of the tissue layers (Figure 9I-O). Their primary functional targets are the detrusor muscle (Figure 9J), urothelium (Figure 9N,O) and vasculature (Figure 9L-M). Nerves are also found on the outer surface of the bladder (serosa and adventitia) and in the lamina propria as they pass through to their final target cells in the urothelium or blood vessels. The detrusor is evenly innervated throughout its depth but the urothelium is more densely innervated in the basal layer, with relatively few axons entering the intermediate and

superficial layers (Figure 9N). At a macroscopic level there is also a pronounced gradient of urothelial innervation, with many more urothelial nerves present within the bladder neck and pelvic urethra compared with the bladder fundus (or dome) (Figure 9O). The pelvic urethra shows a similar pattern of innervation as the bladder, although the urothelium has a higher density of axons (Figure 9P) and a more pronounced muscularis mucosa in which nerves can be found.

Sensory axons arise from lumbar and sacral dorsal root ganglia that lie close to the spinal cord, whereas most of the autonomic axons in the LUT arise from pelvic ganglia that lie very close to the urogenital organs (Figure 9G-HQ-S). A small number of autonomic neuronal cell bodies are also embedded in the outer wall of the bladder neck and form intramural ganglia (Figure 9S), although they are less common than reported in guinea pig, pig and human bladder (Dixon et al., 1983; Gabella, 1990; Gillespie et al., 2006; Pirker et al., 2005). Sensory and autonomic axons travel together in large bundles of hundreds of axons as they enter the organs of the LUT, and then branch into smaller bundles of axons, finally separating to single axons in their target tissue. Although larger bundles of axons can be seen in conventional histology preparations, the small diameter of a single axon (just a few microns or less) precludes visualization of individual axons, so they are typically assessed using immunohistochemistry or reporter mice. As in other organs, the part of the axon that is further from its termination (i.e. within larger bundles of multiple axons) is typically smooth (non-varicose), whereas in the final segment of the axon there are small, regularly spaced swellings (varicosities) (shown in Figure 9J). Varicosities are sites of neurotransmitter storage and release.

Pelvic ganglia

Pelvic ganglia are much larger in adult males, primarily due to the greater number of sympathetic neurons that innervate the male internal reproductive organs (Keast, 2006). In the embryo, when reproductive organs are still developing, the paired pelvic ganglia are closely opposed to the dorsolateral surface of the bladder neck and extend to the anterior PLUR (Figure 9D-HQ-S). However, as reproductive organs enlarge, their spatial relationship begins to change, having close proximity to the prostate gland in males and the uterine cervix in females. During this period of development, the compact pelvic ganglia also begin to become thinner and more dispersed across a broader area, such that discontinuities between regions of ganglia appear and some boundaries can be difficult to identify.

The pelvic ganglia provide all of the parasympathetic and most of the sympathetic innervation to lower urinary tract, distal colon and rectum, and reproductive tract. Most pelvic ganglion neurons innervate targets on the same side of the animal, but there is a small amount of contralateral innervation, and some crossing of axons between the dorsal aspects of the ganglia (Figure 9H). Numerous axon bundles emerge from consistent locations of the pelvic ganglia and comprise connections with the lumbar and sacral spinal dorsal root ganglia and spinal cord (hypogastric and pelvic nerves, respectively), and postganglionic axons projecting to specific targets (e.g. the cavernous nerve innervating erectile tissue of the penis; rectal nerves innervating the distal colon, rectum and internal anal sphincter). Most of these nerves contain both sensory and motor axons.

ABBREVIATIONS AND ACRONYMS

apbl, adventitia of primitive bladder

aplur, adventitia of pelvic urethra of M/F

apr, anterior prostate bud

aprgl, anterior prostate gland

aprur, adventitia of prostatic urethra

amp, anterior mesenchymal pad of M/F

BL, bladder

bugl, bulbourethral gland of M/F (syn: Bartholin's glands in F)

cc, corpus cavernosum

CL, cloaca

clam, cloaca associated mesenchyme

cle, cloacal epithelium (syn: cloacal endoderm)

CLUR, clitoral urethra

cnd, common nephric duct (syn: common mesonephric duct)

CUGS, caudal urogenital sinus (syn: primitive pelvic urethra)

dd, ductus deferens (syn: vas deferens)

dev.vas, developing vasculature of M/F GT

dgt, distal genital tubercle of M/F

dgs, dorsal genital swelling (syn: anterior genital swelling, dorsal genital tubercle)

dmbl, detrusor muscle of bladder (syn: smooth muscle layer of)

dmp, dorsal mesenchymal pad of M/F

dpr, dorsal prostate bud

dprgl, dorsal prostate gland

eclur, epithelium of clitoral urethra

ed, ejaculatory duct

ephur, epithelium of phallic urethra of M/F

epnur, epithelium of penile urethra

eprur, epithelium of prostatic urethra

eugs, epithelium of UGS

gl, glans of M/F GT

glcl, glans clitoris

glgt, glans of M/F gt

glp, glans penis (syn: penile glans)

go, gonad

GT, genital tubercle (of M/F) (syn: penis anlage / clitoris anlage)

gtm, genital tubercle mesenchyme of M/F

hg, hindgut

IC, intermediate cells of bladder urothelium

impbl, inner mesenchymal layer of primitive bladder (syn: suburothelial mesenchyme of)

Krt5-BC, Krt5-basal cells of bladder urothelium (syn: K5-basal cells of)

lpbl, lamina propria of bladder

lplur, lamina propria of PLUR of M/F

lpr, lateral prostate bud

lprgl, lateral prostate gland

lprur, lamina propria of prostatic urethra;

LSW, labial swelling

mdgt, mesenchyme of distal GT of M/F

mes, mesonephros

mgl, mesenchyme of glans of M/F GT

mlplur, mesenchymal layer of PLUR of M/F

mlprur, mesenchymal layer of prostatic urethra

mm, metanephric mesenchyme

mmplur, muscularis mucosa of PLUR of M/F

mmprur, muscularis mucosa of prostatic urethra

mpbl, mesenchyme of primitive bladder (syn: primitive bladder mesenchyme)

mpgt, mesenchyme of proximal genital tubercle of M/F

mpps, mesenchyme of M/F preputial swelling

mt, mesonephric tubule

mugs, mesenchyme of UGS

MUMP, male urogenital mating protuberance

MUMP rg, MUMP ridge groove;

mupbl, muscle layer of primitive bladder (syn: smooth muscle layer of)

muplur, muscle layer of PLUR of M/F

muprur, muscle layer of prostatic urethra

nd, nephric duct of M/F (syn: mesonephric duct, Wolffian duct)

olbl, outer layer of bladder

olpbl, outer lamina propria of bladder (syn: muscularis mesenchyme of)

ompbl, outer mesenchymal layer of primitive bladder (syn: peripheral mesenchyme of)

ov, ovary

PBL, primitive bladder (syn: cranial urogenital sinus)

pc, peritoneal cavity

pce, prepuce of M/F (from TS25 in F syn: clitoral hood)

pgt, proximal genital tubercle of M/F

PHUR, phallic urethra of M/F

PLUR, pelvic urethra of M/F

pnd, paramesonephric duct of M/F (syn: Mullerian duct)

pps, preputial swelling of M/F

PNUR, penile urethra

pr, prostate gland

prgl, preputial gland of M/F

PRUR, prostatic urethra

prox ur me, proximal urethral meatus of M/F (syn: urethral duct, proximal urethral opening)

sbl, serosa of bladder

SC, superficial cells of bladder urothelium (syn: umbrella cells of)

scr fold, scotal fold

scr swell, scrotal swelling

segt, surface ectoderm of gt

smplur, submucosa of PLUR of M/F

smprur, submucosa of prostatic urethra

spbl, serosa of primitive bladder

SSW, scrotal swelling

sulpbl, suburothelial lamina propria of bladder (syn: suburothelial stroma of)

sv, seminal vesicle (syn: vesicular gland, vesicular seminalis)

svb, sinovagnial bulb

t, testis

tg, tailgut

ub, ureteric bud

ubl, urothelium of bladder (syn: epithelium of primitive bladder)

ugbud, urethral gland bud of M/F

ugm, urogenital membrane of M/F

UGS, urogenital sinus

UGS ridge, urogenital sinus ridge (of M/F) (syn: sinus ridge)

upbl, urothelium of primitive bladder

upe, urethral plate epithelium (of M/F) (syn: urethral plate)

ur, ureter

ur gland, M/F urethral gland

uro ureter, urothelium of ureter

urs, urorectal septum

urseam, urethral seam

ute, urethral tube epithelium of M/F

uv, upper vagina

veb, ventral epithelial bud of M/F

ver, verumontanum (syn: seminal colliculus)

vlgs, ventrolateral genital swelling (syn: lateral plate mesoderm buds, ventrolateral genital tubercle)

vmp, ventral mesenchymal pad of M/F

vpr, ventral prostate bud

vprgl, ventral prostate gland

Table 1 Transgenic Mouse Strains

Allele	Strain name in text	Background strain	Figure	Source and Reference(s)
Tg(Hoxb7-EGFP)	*Hoxb7GFP*	mixed background; Swiss Webster were crossed to *Tg(Hoxb7-EGFP)*	1I-M, 4D, 6K	Sourced from and generated by Constantini lab, Columbia University, USA (Srinivas et al., 1999; Rosselot et al., 2010).
Gli1tm2Alj/J	*Gli1-lacZ*	mixed background; Swiss Webster were crossed to *Gli1tm2Alj/J*	7E, F, I, J	Sourced from the Jackson Labs (Ahn and Joyner, 2004).
Up2-Cfp	*Up2-Cfp*	mixed background; Swiss Webster were crossed to *Up2-Cfp*	8N	Generated by Mendelsohn lab, Columbia University, USA (Gandhi et al., 2013).
Shh$^{tm1(eGFP-Cre)}$ GtRosa26^{tm1Sor}	*ShhGFPCre; R26 lacZ*	mixed background; CD1 females were crossed to males carrying the *ShhGFPcre;R26RlacZ* allele (B6.Cg-Shhtm1(EGFP/cre)Cjt/J)	2F, 3A-L, 3U-V	*ShhGFPcre* and *Rosa26R^{lacZ}* (Soriano, 1999; Sun et al., 2000; Harfe et al., 2004). Cell lineage maps in the LUT using the *ShhGFPcre* and *Rosa26R^{lacZ}* strains have been described (Seifert, et al., 2008).

Table 2 Primary Antibodies

Antigen	Name(s)	MGI gene symbol	Species	Supplier	Catalogue Number	Dilution	Figure
Acta1	actin alpha-skeletal muscle	Acta1	Mouse (monoclonal)	Life Technologies	180177	1:250	5J
Acta2	actin alpha-smooth muscle	Acta2	Mouse (monoclonal)	Leica Microsystems	SMA-CE	1:250	5J, 8R
Acta2	actin alpha-smooth muscle	Acta2	Mouse (monoclonal)	Dako, Carpinteria, CA	M0851	1:100	5CG,6G-L,7GHK
β-catenin	catenin beta 1	Ctnnb1	Mouse (monoclonal)	BD Transduction labs	610153	1:100	1H
Cdh1	cadherin 1 (E-cadherin)	Cdh1	Rabbit (monoclonal)	Cell Signaling Technologies, Inc.	3195	1:1500	5BFJ, 8R
Cdh1	cadherin 1 (E-cadherin)	Cdh1	Goat (polyclonal)	R&D	AF748	1:400	1EFGIJ
CGRP	calcitonin/calcitonin-related polypeptide, alpha, (calcitonin gene-related peptide)	Calca	Goat (polyclonal)	AbD Serotec	1720-9007	1:2000	9KOP
FoxA2	forkhead box A2	FoxA2	Rabbit (polyclonal)	Seven Hills	WRAB-FOXA2	1:1000	8U
Hu	ELAV (embryonic lethal, abnormal vision, Drosophila)-like 4, (Hu antigen D, HuD)	Elavl4	Human	gift of V. Lennon	n/a	1:10000	9QS
Krt13	keratin 13	Krt13	Rabbit (polyclonal)	LSBio	c105651	1:400	5L
Krt13	keratin 13	Krt13	Rabbit (polyclonal)	LSBio	LS-B10431/49125	1:100	8VX
Krt14	keratin 14	Krt14	Rabbit (polyclonal)	Covance	Prb 155-P	1:500	8SW
Krt5	keratin 5	Krt5	Chicken (polyclonal)	Covance	SIG-3475-100	1:500	8G-LNSUWX
Laminin	laminin, (pan-laminin)	Laminin	Rabbit	Sigma	L-9393	1:200	1DKLM,7IJ

			(polyclonal)				
Pax2	paired box 2	Pax2	Rabbit (polyclonal)	Zymed	716000	1:70	4H
Pecam1	platelet/endothelial cell adhesion molecule 1 (Cd31)	Pecam1	Rat (monoclonal)	BDPharmingen	557355	1:1000	9M
PGP9.5	ubiquitin carboxy-terminal hydrolase L1	Uchl1	Rabbit (polyclonal)	AbD Serotec	7863-0504	1:4000	9LMQ
PGP9.5	ubiquitin carboxy-terminal hydrolase L1	Uchl1	Rabbit (polyclonal)	Chemicon/Millipore	CAB5925	1:2000	9IN
TH	tyrosine hydroxylase	Th	Rabbit (polyclonal)	Chemicon/Millipore	AB152	1:2000	9L
Trp63	transformation related protein 63, (p63)	Trp63	Rabbit (polyclonal)	GenTEX	GTX102425	1:300	4H,5MN,8G-NSUV
Upk	uroplakin, (pan-uroplakin)	Upk	Mouse (monoclonal)	Fitzgerald	10R-U103a	1:50	5CGL-N,6G-JL,7GHK,8MV
VAChT	solute carrier family 18 (vesicular monoamine), member 3, (VAT)	Slc18a3	Rabbit (polyclonal)	Synapic Systems	139 103	1:1000	9GHR
VAChT	solute carrier family 18 (vesicular monoamine), member 3, (VAT)	Slc18a3	Goat (polyclonal)	Chemicon/Millipore	ABN100	1:1000	9J

SUPPLEMENTARY FIGURES

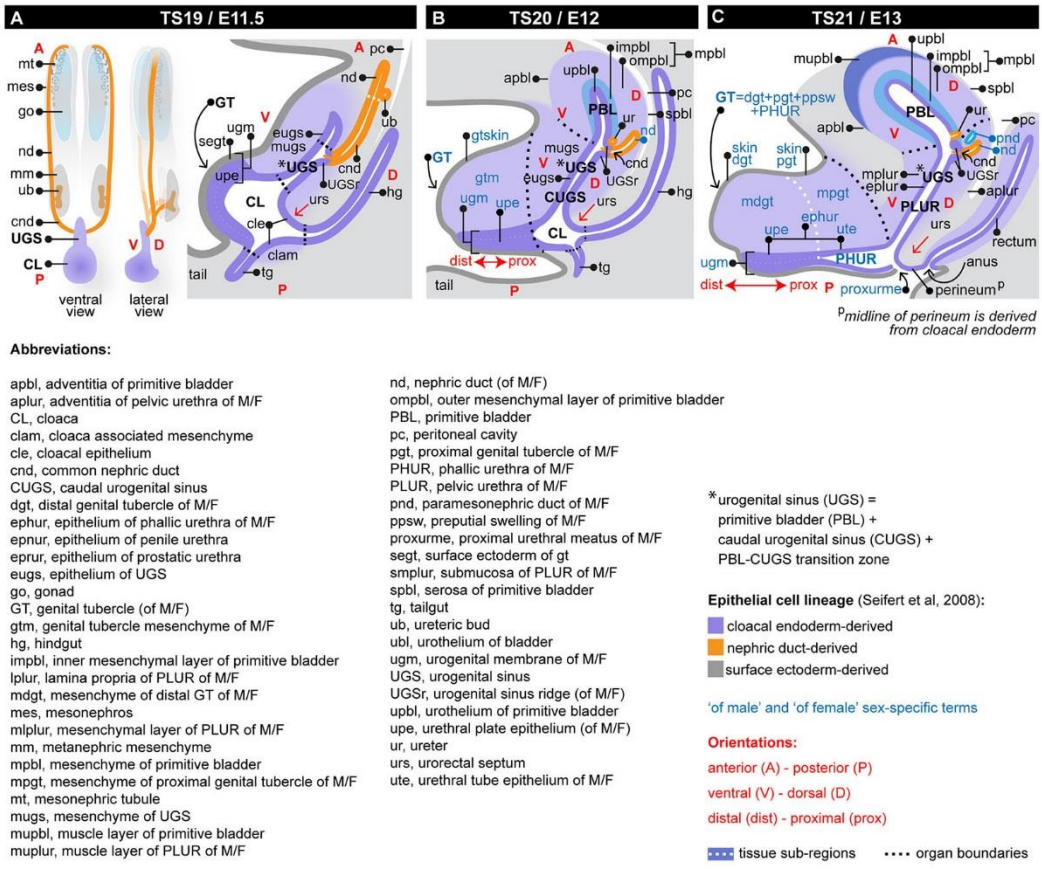

Supplementary Figure 1. Urogenital sinus development. Schematics illustrate early development. Three-dimensional views (**A**) and representative sagittal sections at the mid-line (**B-C**) are shown. Red arrows (**A-C**) indicate direction of mesenchymal growth, resulting in separation of the hindgut and UGS. Supplementary to Figure 1.

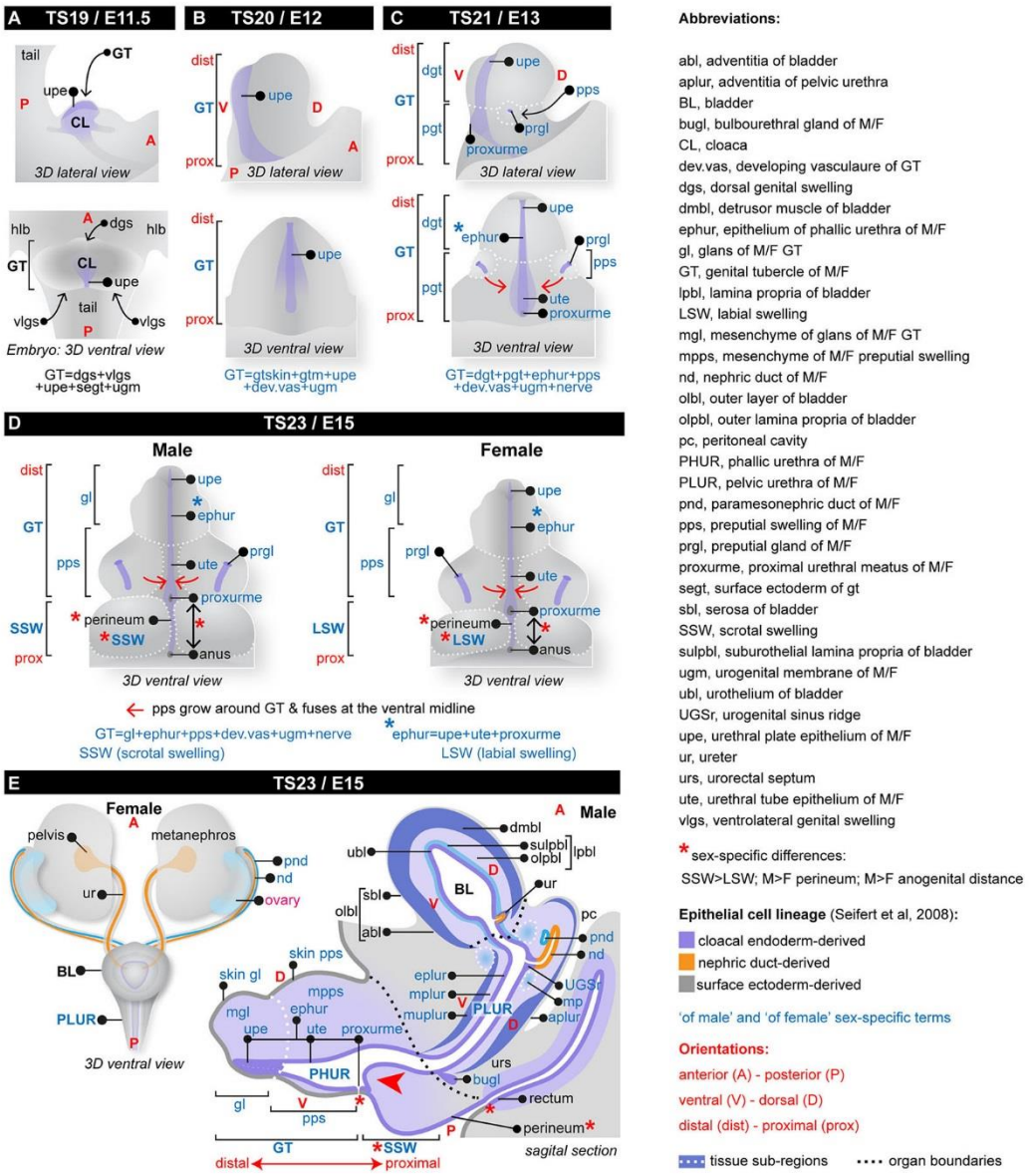

Supplementary Figure 2. Genital tubercle development. Schematics illustrate GT development. Red arrows (**C-D**) indicate direction of preputial swelling growth; towards the ventral midline of the genital tubercle. Red arrowhead (in **E**) indicates direction of mesenchymal growth seen in males, which begins to septate the epithelium of the PHUR (ephur). Supplementary to Figure 2.

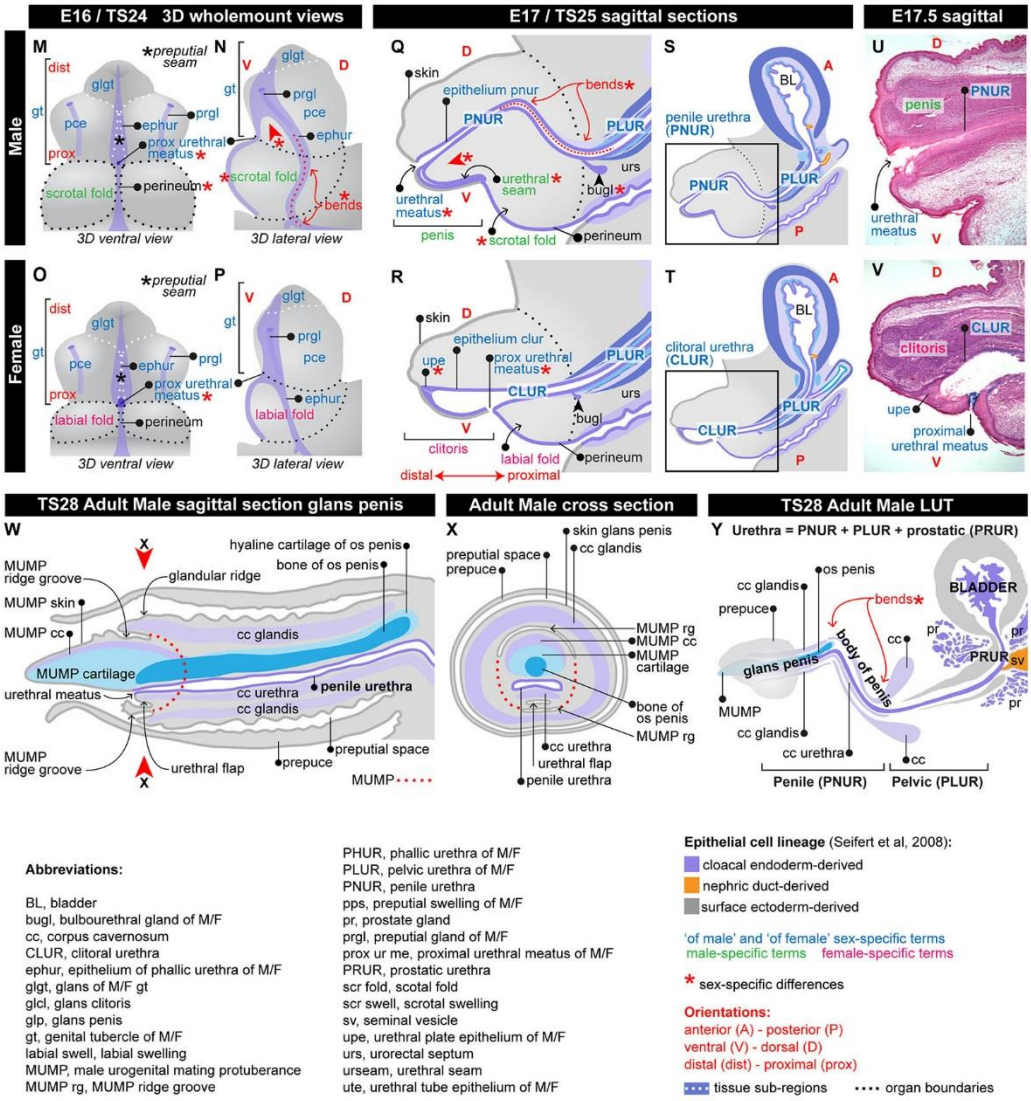

Supplementary Figure 3. Sexual differentiation of the external genitalia. Schematics illustrate external genitalia. Red arrowheads in **N** and **Q** show direction of mesenchymal growth seen in males and epithelium of the penile urethra (PNUR) septation. Red arrows in **N**, **Q** and **Y** show the location of two right angle bends in the male urethra; at the glans-body junction of the penis and the penile urethra-pelvic urethra junction. Red arrowheads in **W** indicate position of cross section (**X**). Supplementary to Figure 3.

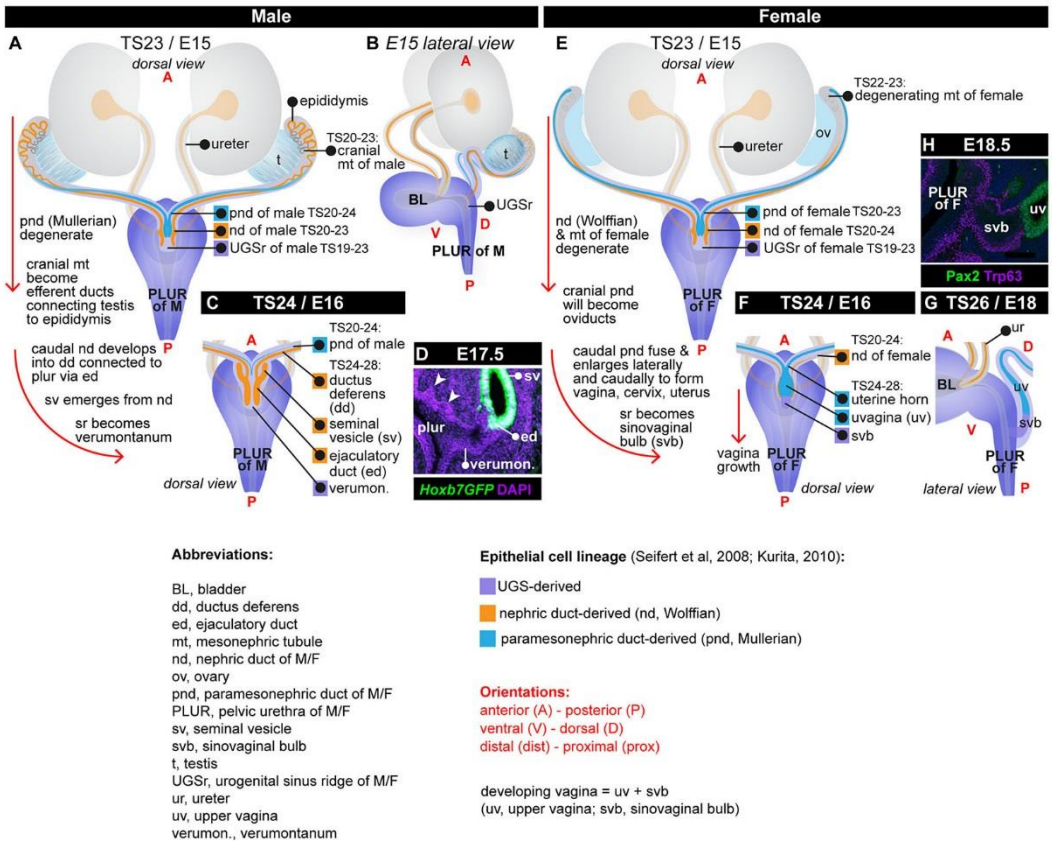

Abbreviations:

BL, bladder
dd, ductus deferens
ed, ejaculatory duct
mt, mesonephric tubule
nd, nephric duct of M/F
ov, ovary
pnd, paramesonephric duct of M/F
PLUR, pelvic urethra of M/F
sv, seminal vesicle
svb, sinovaginal bulb
t, testis
UGSr, urogenital sinus ridge of M/F
ur, ureter
uv, upper vagina
verumon., verumontanum

Epithelial cell lineage (Seifert et al, 2008; Kurita, 2010):

UGS-derived
nephric duct-derived (nd, Wolffian)
paramesonephric duct-derived (pnd, Mullerian)

Orientations:
anterior (A) - posterior (P)
ventral (V) - dorsal (D)
distal (dist) - proximal (prox)

developing vagina = uv + svb
(uv, upper vagina; svb, sinovaginal bulb)

Supplementary Figure 4. Sexual differentiation of the reproductive ducts. Schematics illustrate 3-dimensional anatomy of the reproductive ducts and their connection to the pelvic urethra (PLUR). Red arrows in **A** and **E** indicate major anatomical changes that occur from TS23 to TS24. White arrows in **D** indicate anterior prostate buds. Red arrow in **F** indicates direction of vaginal growth. Supplementary to Figure 4.

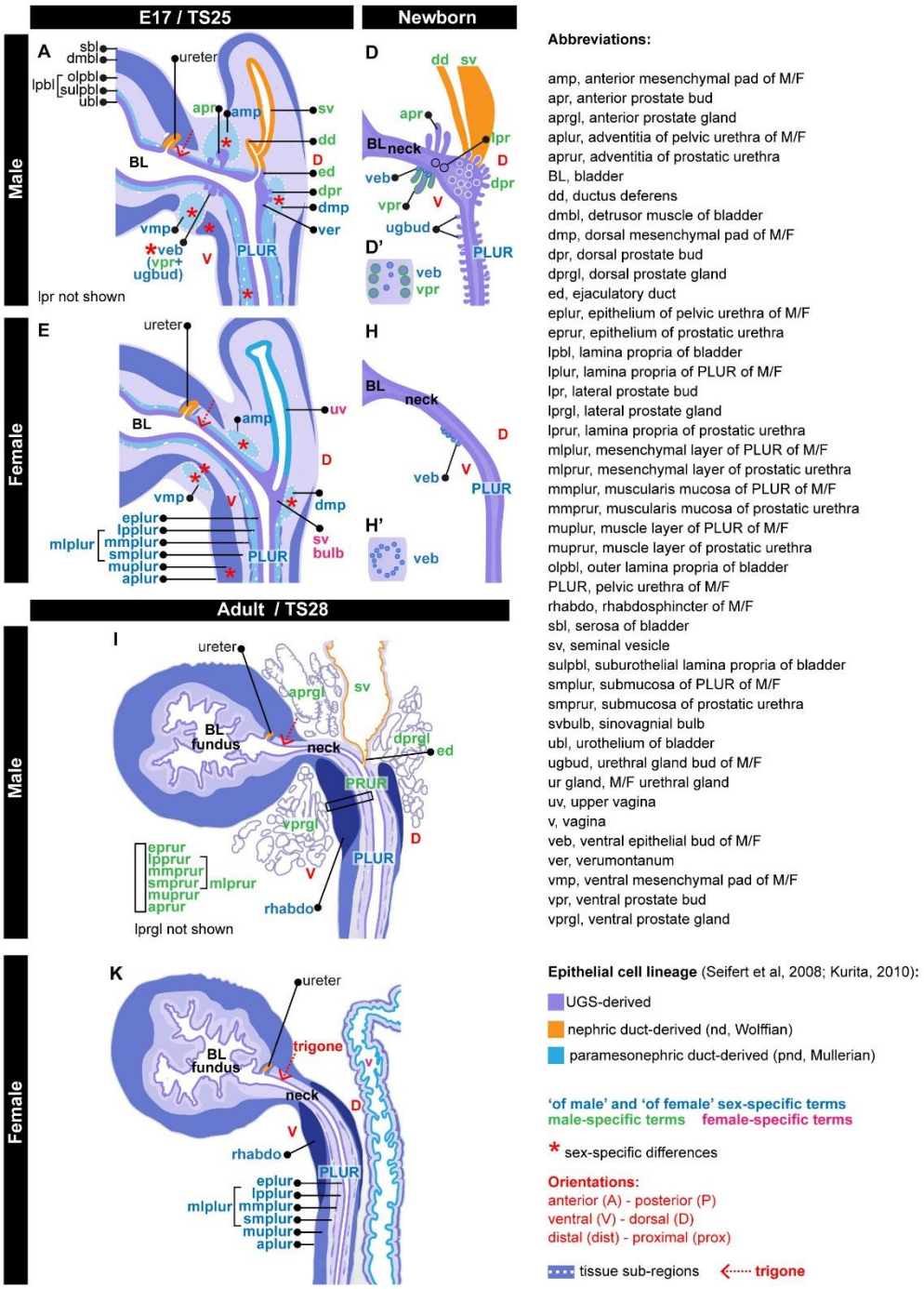

Supplementary Figure 5. Sexual differentiation of the pelvic urethra. Schematics illustrate midline, sagittal sections of the bladder-pelvic urethra junction at E17 (**A, E**) and adult (**I, K**) and three-dimensional views of the PLUR epithelium (purple) at birth (**D, H**). Underside views of ventral PLUR epithelium are shown in **D'** and **H'**. Black rectangles in **I** show the tissue layers present in the prostatic urethra (PRUR). Supplementary to Figure 5.

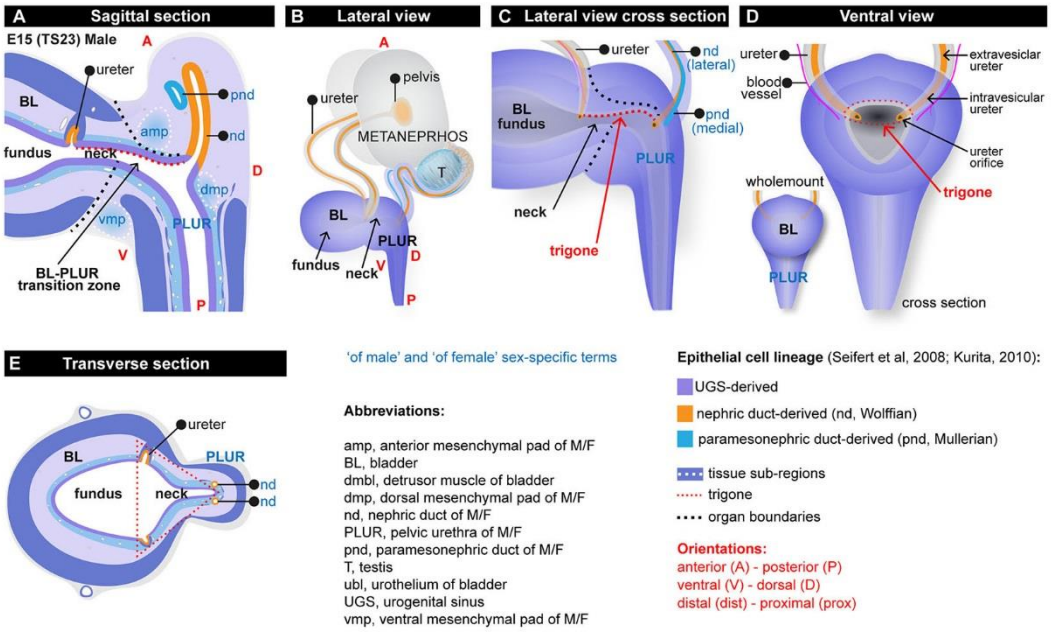

Supplementary Figure 6. Morphology of the bladder fundus, neck, trigone and ureters. Schematics illustrate the location and morphology of the bladder regions and ureter and urethra connections at E15. Supplementary to Figure 6.

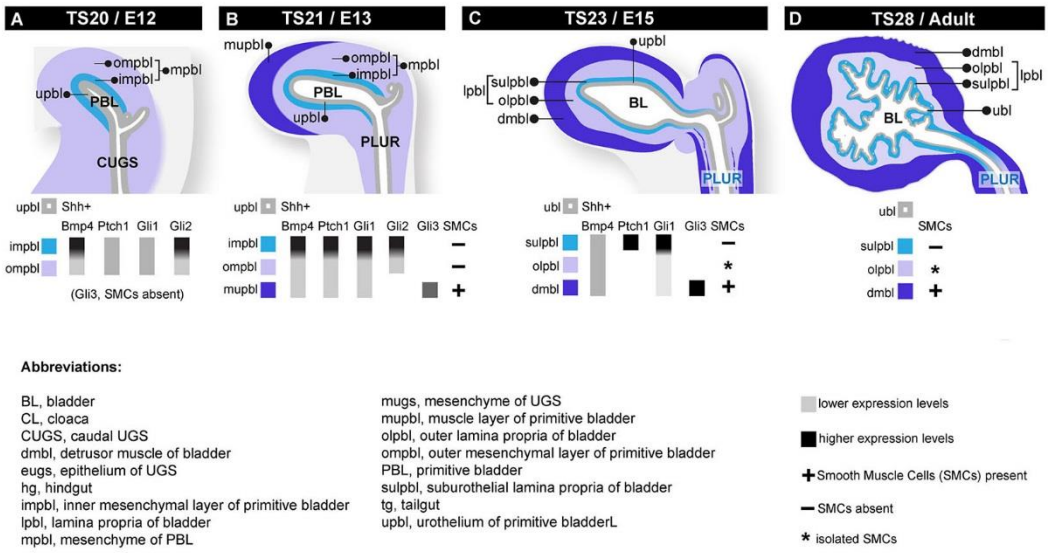

Abbreviations:

BL, bladder
CL, cloaca
CUGS, caudal UGS
dmbl, detrusor muscle of bladder
eugs, epithelium of UGS
hg, hindgut
impbl, inner mesenchymal layer of primitive bladder
lpbl, lamina propria of bladder
mpbl, mesenchyme of PBL
mugs, mesenchyme of UGS
mupbl, muscle layer of primitive bladder
olpbl, outer lamina propria of bladder
ompbl, outer mesenchymal layer of primitive bladder
PBL, primitive bladder
sulpbl, suburothelial lamina propria of bladder
tg, tailgut
upbl, urothelium of primitive bladderL

lower expression levels
higher expression levels
+ Smooth Muscle Cells (SMCs) present
– SMCs absent
* isolated SMCs

Supplementary Figure 7. Radial patterning of the bladder mesenchyme. Schematics representing midline sagittal sections, illustrate mesenchymal and smooth muscle layers of the primitive bladder (PBL) and bladder (BL). Supplementary to Figure 7.

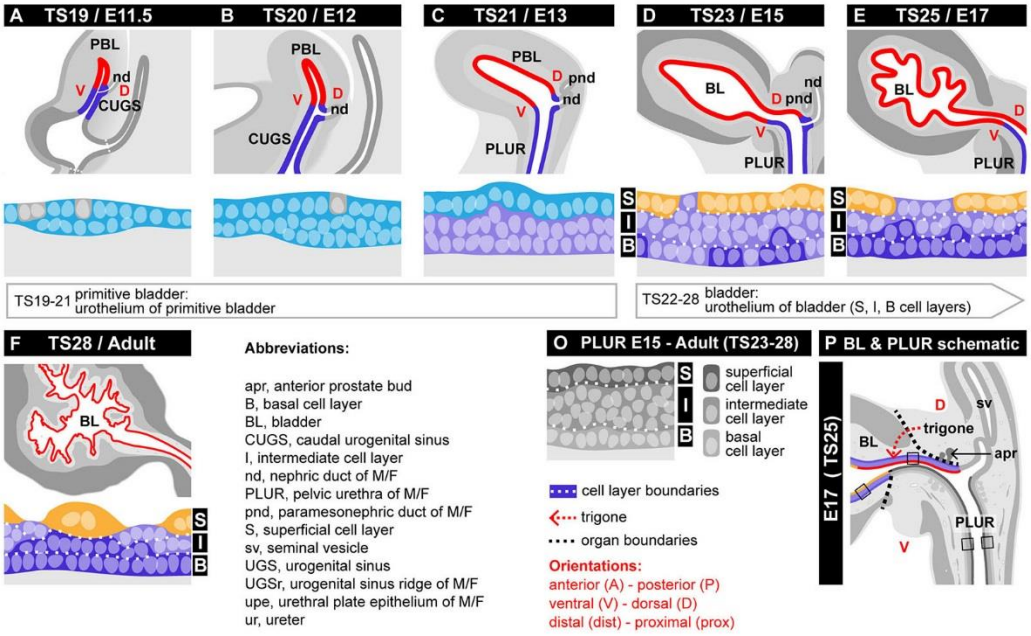

Supplementary Figure 8. The bladder urothelium and PLUR epithelium cell types. A-F: Schematics illustrate midline sagittal sections. The epithelial layers are highlighted; urothelium of primitive bladder/bladder (PBL/BL) in red and epithelium of caudal urogenital sinus/pelvic urethra (CUGS/PLUR) in blue. Below, cross sections illustrate location and gene expression of urothelial cell types seen in the primitive bladder/bladder. **O-P:** PLUR schematics; a cross section illustrates the epithelial layers of the PLUR (**O**) and a sagittal section of the bladder-PLUR boundary at E17 (**P**). In **O-P**: epithelium of PLUR layers are shown in different shades of grey. In **P**: the urothelium of bladder layers are shown in red (superficial cell layer of urothelium of trigone), yellow (superficial cell layer of urothelium), light purple (intermediate cell layer of urothelium), and dark purple (basal cell layer of urothelium). Supplementary to Figure 8.

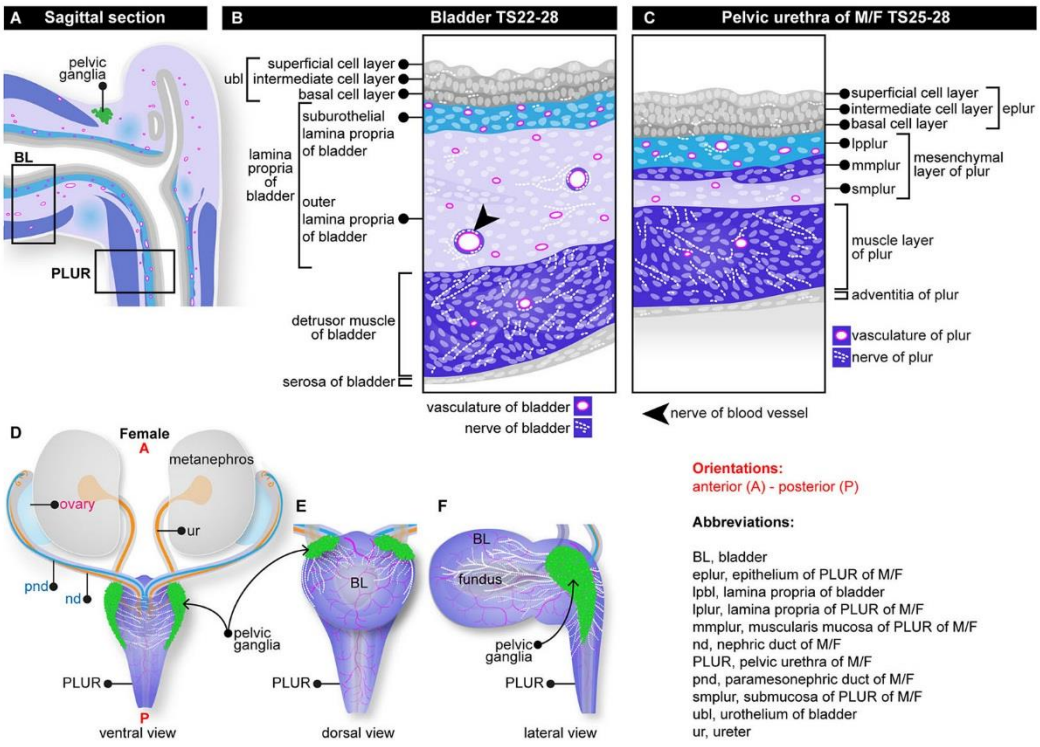

Supplementary Figure 9. Nerves, pelvic ganglia and vasculature of the LUT. Schematics illustrate nerves, pelvic ganglia and vasculature. Schematics are representative of sagittal sections (**A-C**) and three-dimensional views of the urogenital system (**D**) and bladder/pelvic urethra (**E-F**) at E15. Supplementary to Figure 9.

SUPPLEMENTARY REFERENCES

Abler, L.L., Keil, K.P., Mehta, V., Joshi, P.S., Schmitz, C.T., Vezina, C.M. (2011). A high-resolution molecular atlas of the fetal mouse lower urogenital tract. *Dev Dyn* **240**, 2364-2377.

Ahn, S., Joyner, A.L. (2004). Dynamic changes in the response of cells to positive hedgehog signaling during mouse limb patterning. *Cell* **118**, 505-516.

Allgeier, S.H., Lin, T.M., Moore, R.W., Vezina, C.M., Abler, L.L., Peterson, R.E. (2010). Androgenic regulation of ventral epithelial bud number and pattern in mouse urogenital sinus. *Dev Dyn* **239**, 373-385.

Allgeier, S.H., Lin, T.M., Vezina, C.M., Moore, R.W., Fritz, W.A., Chiu, S.Y., Zhang, C., Peterson, R.E. (2008). WNT5A selectively inhibits mouse ventral prostate development. *Dev Biol* **324**, 10-17.

Batourina, E., Tsai, S., Lambert, S., Sprenkle, P., Viana, R., Dutta, S., Hensle, T., Wang, F., Niederreither, K., McMahon, A.P., et al. (2005). Apoptosis induced by vitamin A signaling is crucial for connecting the ureters to the bladder. *Nat Genet* **37**, 1082-1089.

Biancardi, M.F., Santos, F.C., Madi-Ravazzi, L., Goes, R.M., Vilamaior, P.S., Felisbino, S.L., Taboga, S.R. (2010). Testosterone promotes an anabolic increase in the rat female prostate (Skene's paraurethral gland) which acquires a male ventral prostate phenotype. *Anat Rec (Hoboken)* **293**, 2163-2175.

Birder, L.A. (2011). Urothelial signaling. *Handb Exp Pharmacol*, 207-231.

Birder, L.A., de Groat, W.C. (2007). Mechanisms of disease: involvement of the urothelium in bladder dysfunction. *Nat Clin Pract Urol* **4**, 46-54.

Blaschko, S.D., Mahawong, P., Ferretti, M., Cunha, T.J., Sinclair, A., Wang, H., Schlomer, B.J., Risbridger, G., Baskin, L.S., Cunha, G.R. (2013). Analysis of the effect of estrogen/androgen perturbation on penile development in transgenic and diethylstilbestrol-treated mice. *Anat Rec (Hoboken)* **296**, 1127-1141.

Carpenter, A., Paulus, A., Robinson, M., Bates, C.M., Robinson, M.L., Hains, D., Kline, D., McHugh, K.M. (2012). 3-Dimensional morphometric analysis of murine bladder development and dysmorphogenesis. *Dev Dyn* **241**, 522-533.

Chia, I., Grote, D., Marcotte, M., Batourina, E., Mendelsohn, C., Bouchard, M. (2011). Nephric duct insertion is a crucial step in urinary tract maturation that is regulated by a Gata3-Raldh2-Ret molecular network in mice. *Development* **138**, 2089-2097.

Cohn, M.J. (2011). Development of the external genitalia: conserved and divergent mechanisms of appendage patterning. *Dev Dyn* **240**, 1108-1115.

Cunha, G.R., Donjacour, A.A., Cooke, P.S., Mee, S., Bigsby, R.M., Higgins, S.J., Sugimura, Y. (1987). The endocrinology and developmental biology of the prostate. *Endocr Rev* **8**, 338-362.

Dixon, J.S., Gilpin, S.A., Gilpin, C.J., Gosling, J.A. (1983). Intramural ganglia of the human urinary bladder. *Br J Urol* **55**, 195-198.

Donjacour, A.A., Cunha, G.R., Sugimura, Y. (1987). Heterogeneity of structure and function in the mouse prostate. *Prog Clin Biol Res* **239**, 583-600.

Erman, A., Veranic, P., Psenicnik, M., Jezernik, K. (2006). Superficial cell differentiation during embryonic and postnatal development of mouse urothelium. *Tissue Cell* **38**, 293-301.

Feeney, M.M., Rosenblum, N.D. (2014). Urinary tract pacemaker cells: current knowledge and insights from nonrenal pacemaker cells provide a basis for future discovery. *Pediatr Nephrol* **29**, 629-635.

Fochi, R.A., Perez, A.P., Bianchi, C.V., Rochel, S.S., Goes, R.M., Vilamaior, P.S., Taboga, S.R., Santos, F.C. (2008). Hormonal oscillations during the estrous cycle influence the morphophysiology of the gerbil (Meriones unguiculatus) female prostate (skene paraurethral glands). *Biol Reprod* **79**, 1084-1091.

Gabella, G. (1990). Intramural neurons in the urinary bladder of the guinea-pig. *Cell Tissue Res* **261**, 231-237.

Gabella, G. (1995). The structural relations between nerve fibres and muscle cells in the urinary bladder of the rat. *J Neurocytol* **24**, 159-187.

Gabella, G. (1999). Structure of the intramural nerves of the rat bladder. *J Neurocytol* **28**, 615-637.

Gabella, G., Davis, C. (1998). Distribution of afferent axons in the bladder of rats. *J Neurocytol* **27**, 141-155.

Gandhi, D., Molotkov, A., Batourina, E., Schneider, K., Dan, H., Reiley, M., Laufer, E., Metzger, D., Liang, F., Liao, Y., et al. (2013). Retinoid signaling in progenitors controls specification and regeneration of the urothelium. *Dev Cell* **26**, 469-482.

Gillespie, J.I., Markerink-van Ittersum, M., de Vente, J. (2006). Sensory collaterals, intramural ganglia and motor nerves in the guinea-pig bladder: evidence for intramural neural circuits. *Cell Tissue Res* **325**, 33-45.

Haraguchi, R., Mo, R., Hui, C., Motoyama, J., Makino, S., Shiroishi, T., Gaffield, W., Yamada, G. (2001). Unique functions of Sonic hedgehog signaling during external genitalia development. *Development* **128**, 4241-4250.

Haraguchi, R., Motoyama, J., Sasaki, H., Satoh, Y., Miyagawa, S., Nakagata, N., Moon, A., Yamada, G. (2007). Molecular analysis of coordinated bladder and urogenital organ formation by Hedgehog signaling. *Development* **134**, 525-533.

Haraguchi, R., Suzuki, K., Murakami, R., Sakai, M., Kamikawa, M., Kengaku, M., Sekine, K., Kawano, H., Kato, S., Ueno, N., et al. (2000). Molecular analysis of external genitalia formation: the role of fibroblast growth factor (Fgf) genes during genital tubercle formation. *Development* **127**, 2471-2479.

Harfe, B.D., Scherz, P.J., Nissim, S., Tian, H., McMahon, A.P., Tabin, C.J. (2004). Evidence for an expansion-based temporal Shh gradient in specifying vertebrate digit identities. *Cell* **118**, 517-528.

Hashitani, H., Mitsui, R., Shimizu, Y., Higashi, R., Nakamura, K. (2012). Functional and morphological properties of pericytes in suburothelial venules of the mouse bladder. *Br J Pharmacol* **167**, 1723-1736.

Hoshi, M., Batourina, E., Mendelsohn, C., Jain, S. (2012). Novel mechanisms of early upper and lower urinary tract patterning regulated by RetY1015 docking tyrosine in mice. *Development* **139**, 2405-2415.

Hossler, F.E., Lametschwandtner, A., Kao, R., Finsterbusch, F. (2013). Microvascular architecture of mouse urinary bladder described with vascular corrosion casting, light microscopy, SEM, and TEM. *Microsc Microanal* **19**, 1428-1435.

Hu, P., Meyers, S., Liang, F.X., Deng, F.M., Kachar, B., Zeidel, M.L., Sun, T.T. (2002). Role of membrane proteins in permeability barrier function: uroplakin ablation elevates urothelial permeability. *Am J Physiol Renal Physiol* **283**, F1200-1207.

Huang, C.C., Orvis, G.D., Kwan, K.M., Behringer, R.R. (2014). Lhx1 is required in Mullerian duct epithelium for uterine development. *Dev Biol* **389**, 124-136.

Hutch, J.A. (1972). Anatomy and physiology of the bladder, trigone and urethra. London, New York,: Butterworths Appleton-Century-Crofts.

Iizuka-Kogo, A., Ishidao, T., Akiyama, T., Senda, T. (2007). Abnormal development of urogenital organs in Dlgh1-deficient mice. *Development* **134**, 1799-1807.

Inoue, T., Gabella, G. (1991). A vascular network closely linked to the epithelium of the urinary bladder of the rat. *Cell Tissue Res* **263**, 137-143.

Jost, S.P. (1986). Renewal of normal urothelium in adult mice. *Virchows Arch B Cell Pathol Incl Mol Pathol* **51**, 65-70.

Keast, J.R. (2006). Plasticity of pelvic autonomic ganglia and urogenital innervation. *Int Rev Cytol* **248**, 141-208.

Keil, K.P., Mehta, V., Abler, L.L., Joshi, P.S., Schmitz, C.T., Vezina, C.M. (2012). Visualization and quantification of mouse prostate development by in situ hybridization. *Differentiation* **84**, 232-239.

Khandelwal, P., Abraham, S.N., Apodaca, G. (2009). Cell biology and physiology of the uroepithelium. *Am J Physiol Renal Physiol* **297**, 1477-1501.

Kong, X.T., Deng, F.M., Hu, P., Liang, F.X., Zhou, G., Auerbach, A.B., Genieser, N., Nelson, P.K., Robbins, E.S., Shapiro, E., et al. (2004). Roles of uroplakins in plaque formation, umbrella cell enlargement, and urinary tract diseases. *J Cell Biol* **167**, 1195-1204.

Kurita, T. (2010). Developmental origin of vaginal epithelium. *Differentiation* **80**, 99-105.

Levin, T.L., Han, B., Little, B.P. (2007). Congenital anomalies of the male urethra. *Pediatr Radiol* **37**, 851-862.

Lin, C., Yin, Y., Veith, G.M., Fisher, A.V., Long, F., Ma, L. (2009). Temporal and spatial dissection of Shh signaling in genital tubercle development. *Development* **136**, 3959-3967.

Little, M.H., Brennan, J., Georgas, K., Davies, J.A., Davidson, D.R., Baldock, R.A., Beverdam, A., Bertram, J.F., Capel, B., Chiu, H.S., et al. (2007). A high-resolution anatomical ontology of the developing murine genitourinary tract. *Gene Expr Patterns* **7**, 680-699.

Mackie, G.G., Stephens, F.D. (1975). Duplex kidneys: a correlation of renal dysplasia with position of the ureteral orifice. *J Urol* **114**, 274-280.

Mendelsohn, C. (2009). Using mouse models to understand normal and abnormal urogenital tract development. *Organogenesis* **5**, 306-314.

Miyagawa, S., Moon, A., Haraguchi, R., Inoue, C., Harada, M., Nakahara, C., Suzuki, K., Matsumaru, D., Kaneko, T., Matsuo, I., et al. (2009). Dosage-dependent hedgehog signals integrated with Wnt/beta-catenin signaling regulate external genitalia formation as an appendicular program. *Development* **136**, 3969-3978.

Murawski, I.J., Gupta, I.R. (2008). Gene discovery and vesicoureteric reflux. *Pediatr Nephrol* **23**, 1021-1027.

Murawski, I.J., Myburgh, D.B., Favor, J., Gupta, I.R. (2007). Vesico-ureteric reflux and urinary tract development in the Pax21Neu+/- mouse. *Am J Physiol Renal Physiol*. **293**, 1736-45.

Perriton, C.L., Powles, N., Chiang, C., Maconochie, M.K., Cohn, M.J. (2002). Sonic hedgehog signaling from the urethral epithelium controls external genital development. *Dev Biol* **247**, 26-46.

Pirker, M.E., Montedonico, S., Rolle, U., Austvoll, H., Puri, P. (2005). Regional differences in nitrergic neuronal density in the developing porcine urinary bladder. *Pediatr Surg Int* **21**, 161-168.

Rodriguez, E., Jr., Weiss, D.A., Ferretti, M., Wang, H., Menshenia, J., Risbridger, G., Handelsman, D., Cunha, G., Baskin, L. (2012). Specific morphogenetic events in mouse external genitalia sex differentiation are responsive/dependent upon androgens and/or estrogens. *Differentiation* **84**, 269-279.

Rodriguez, E., Jr., Weiss, D.A., Yang, J.H., Menshenina, J., Ferretti, M., Cunha, T.J., Barcellos, D., Chan, L.Y., Risbridger, G., Cunha, G.R., et al. (2011). New insights on the morphology of adult mouse penis. *Biol Reprod* **85**, 1216-1221.

Rodriguez, I., Araki, K., Khatib, K., Martinou, J.C., Vassalli, P. (1997). Mouse vaginal opening is an apoptosis-dependent process which can be prevented by the overexpression of Bcl2. *Dev Biol* **184**, 115-121.

Romih, R., Korosec, P., de Mello, W., Jr., Jezernik, K. (2005). Differentiation of epithelial cells in the urinary tract. *Cell Tissue Res* **320**, 259-268.

Rosselot, C., Spraggon, L., Chia, I., Batourina, E., Riccio, P., Lu, B., Niederreither, K., Dolle, P., Duester, G., Chambon, P., et al. (2010). Non-cell-autonomous retinoid signaling is crucial for renal development. *Development* **137**, 283-292.

Sasaki, C., Yamaguchi, K., Akita, K. (2004). Spatiotemporal distribution of apoptosis during normal cloacal development in mice. *Anat Rec A Discov Mol Cell Evol Biol* **279**, 761-767.

Schlomer, B.J., Feretti, M., Rodriguez, E., Jr., Blaschko, S., Cunha, G., Baskin, L. (2013). Sexual differentiation in the male and female mouse from days 0 to 21: a detailed and novel morphometric description. *J Urol* **190**, 1610-1617.

Seifert, A.W., Bouldin, C.M., Choi, K.S., Harfe, B.D., Cohn, M.J. (2009a). Multiphasic and tissue-specific roles of sonic hedgehog in cloacal septation and external genitalia development. *Development* **136**, 3949-3957.

Seifert, A.W., Harfe, B.D., Cohn, M.J. (2008). Cell lineage analysis demonstrates an endodermal origin of the distal urethra and perineum. *Dev Biol* **318**, 143-152.

Seifert, A.W., Yamaguchi, T., Cohn, M.J. (2009b). Functional and phylogenetic analysis shows that Fgf8 is a marker of genital induction in mammals but is not required for external genital development. *Development* **136**, 2643-2651.

Seifert, A.W., Zheng, Z., Ormerod, B.K., Cohn, M.J. (2010). Sonic hedgehog controls growth of external genitalia by regulating cell cycle kinetics. *Nat Commun* **1**, 23.

Siiteri, P.K., Wilson, J.D. (1974). Testosterone formation and metabolism during male sexual differentiation in the human embryo. *J Clin Endocrinol Metab* **38**, 113-125.

Sinisi, A.A., Pasquali, D., Notaro, A., Bellastella, A. (2003). Sexual differentiation. *J Endocrinol Invest* **26**, 23-28.

Soriano, P. (1999). Generalized lacZ expression with the ROSA26 Cre reporter strain. *Nat Genet* **21**, 70-71.

Srinivas, S., Goldberg, M.R., Watanabe, T., D'Agati, V., al-Awqati, Q., Costantini, F. (1999). Expression of green fluorescent protein in the ureteric bud of transgenic mice: a new tool for the analysis of ureteric bud morphogenesis. *Dev Genet* **24**, 241-251.

Sun, X., Lewandoski, M., Meyers, E.N., Liu, Y.H., Maxson, R.E., Jr., Martin, G.R. (2000). Conditional inactivation of Fgf4 reveals complexity of signalling during limb bud development. *Nat Genet* **25**, 83-86.

Suzuki, K., Bachiller, D., Chen, Y.P., Kamikawa, M., Ogi, H., Haraguchi, R., Ogino, Y., Minami, Y., Mishina, Y., Ahn, K., et al. (2003). Regulation of outgrowth and apoptosis for the terminal appendage: external genitalia development by concerted actions of BMP signaling [corrected]. *Development* **130**, 6209-6220.

Suzuki, K., Haraguchi, R., Ogata, T., Barbieri, O., Alegria, O., Vieux-Rochas, M., Nakagata, N., Ito, M., Mills, A.A., Kurita, T., et al. (2008). Abnormal urethra formation in mouse models of split-hand/split-foot malformation type 1 and type 4. *Eur J Hum Genet* **16**, 36-44.

Tanagho, E.A. (1981). Devlopment of the Ureter. In *The Ureter*, (ed. Bergman, H.). New York: Springer-Verlag.

Tanagho, E.A., Meyers, F.H., Smith, D.R. (1968). The trigone: anatomical and physiological considerations. I. In relation to the ureterovesical junction. *J Urol* **100**, 623-632.

Timms, B.G. (2008). Prostate development: a historical perspective. *Differentiation* **76**, 565-577.

Timms, B.G., Lee, C.W., Aumuller, G., Seitz, J. (1995). Instructive induction of prostate growth and differentiation by a defined urogenital sinus mesenchyme. *Microsc Res Tech* **30**, 319-332.

Uetani, N., Bertozzi, K., Chagnon, M.J., Hendriks, W., Tremblay, M.L., Bouchard, M. (2009). Maturation of ureter-bladder connection in mice is controlled by LAR family receptor protein tyrosine phosphatases. *J Clin Invest* **119**, 924-935.

Viana, R., Batourina, E., Huang, H., Dressler, G.R., Kobayashi, A., Behringer, R.R., Shapiro, E., Hensle, T., Lambert, S., Mendelsohn, C. (2007). The development of the bladder trigone, the center of the anti-reflux mechanism. *Development* **134**, 3763-3769.

Walker, K.A., Sims-Lucas, S., Di Giovanni, V.E., Schaefer, C., Sunseri, W.M., Novitskaya, T., de Caestecker, M.P., Chen, F., Bates, C.M. (2013). Deletion of fibroblast growth factor receptor 2 from the peri-wolffian duct stroma leads to ureteric induction abnormalities and vesicoureteral reflux. *PLoS One* **8**, e56062.

Weiss, D.A., Rodriguez, E., Jr., Cunha, T., Menshenina, J., Barcellos, D., Chan, L.Y., Risbridger, G., Baskin, L., Cunha, G. (2012). Morphology of the external genitalia of the adult male and female mice as an endpoint of sex differentiation. *Mol Cell Endocrinol* **354**, 94-102.

Weiss, J.P. (1988). Embryogenesis of ureteral anomalies: a unifying theory. *Aust N Z J Surg* **58**, 631-638.

Wernert, N., Albrech, M., Sesterhenn, I., Goebbels, R., Bonkhoff, H., Seitz, G., Inniger, R., Remberger, K. (1992). The 'female prostate': location, morphology, immunohistochemical characteristics and significance. *Eur Urol* **22**, 64-69.

Wiese, C.B., Ireland, S., Fleming, N.L., Yu, J., Valerius, M.T., Georgas, K., Chiu, H.S., Brennan, J., Armstrong, J., Little, M.H., et al. (2012). A genome-wide screen to identify transcription factors expressed in pelvic Ganglia of the lower urinary tract. *Front Neurosci* **6**, 130.

Wu, X., Ferrara, C., Shapiro, E., Grishina, I. (2009a). Bmp7 expression and null phenotype in the urogenital system suggest a role in re-organization of the urethral epithelium. *Gene Expr Patterns* **9**, 224-230.

Wu, X.R., Kong, X.P., Pellicer, A., Kreibich, G., Sun, T.T. (2009b). Uroplakins in urothelial biology, function, and disease. *Kidney Int* **75**, 1153-1165.

Wyndaele, J.J., De Wachter, S. (2003). The basics behind bladder pain: a review of data on lower urinary tract sensations. *Int J Urol* **10 Suppl**, S49-55.

Yamada, G., Satoh, Y., Baskin, L.S., Cunha, G.R. (2003). Cellular and molecular mechanisms of development of the external genitalia. *Differentiation* **71**, 445-460.

Yamada, G., Suzuki, K., Haraguchi, R., Miyagawa, S., Satoh, Y., Kamimura, M., Nakagata, N., Kataoka, H., Kuroiwa, A., Chen, Y. (2006). Molecular genetic cascades for external genitalia formation: an emerging organogenesis program. *Dev Dyn* **235**, 1738-1752.

Yan, H., Keast, J.R. (2008). Neurturin regulates postnatal differentiation of parasympathetic pelvic ganglion neurons, initial axonal projections, and maintenance of terminal fields in male urogenital organs. *J Comp Neurol* **507**, 1169-1183.

Yang, J.H., Menshenina, J., Cunha, G.R., Place, N., Baskin, L.S. (2010). Morphology of mouse external genitalia: implications for a role of estrogen in sexual dimorphism of the mouse genital tubercle. *J Urol* **184**, 1604-1609.

Yiee, J.H., Baskin, L.S. (2010). Penile embryology and anatomy. *ScientificWorldJournal* **10**, 1174-1179.

Yucel, S., Cavalcanti, A.G., Desouza, A., Wang, Z., Baskin, L.S. (2003). The effect of oestrogen and testosterone on the urethral seam of the developing male mouse genital tubercle. *BJU Int* **92**, 1016-1021.

Zaviacic, M., Jakubovska, V., Belosovic, M., Breza, J. (2000). Ultrastructure of the normal adult human female prostate gland (Skene's gland). *Anat Embryol (Berl)* **201**, 51-61.